Near ground surface, engineered structures become unstable in response to extreme changes in moisture flux boundary conditions

CHAPTER 10 MEASUREMENT OF SHEAR STRENGTH PARAMETERS

Design features

Test procedures

Typical results

CHAPTER 10
MEASUREMENT OF SHEAR STRENGTH PARAMETERS

Axis-Translation Technique

Case of No High Air Entry Disk

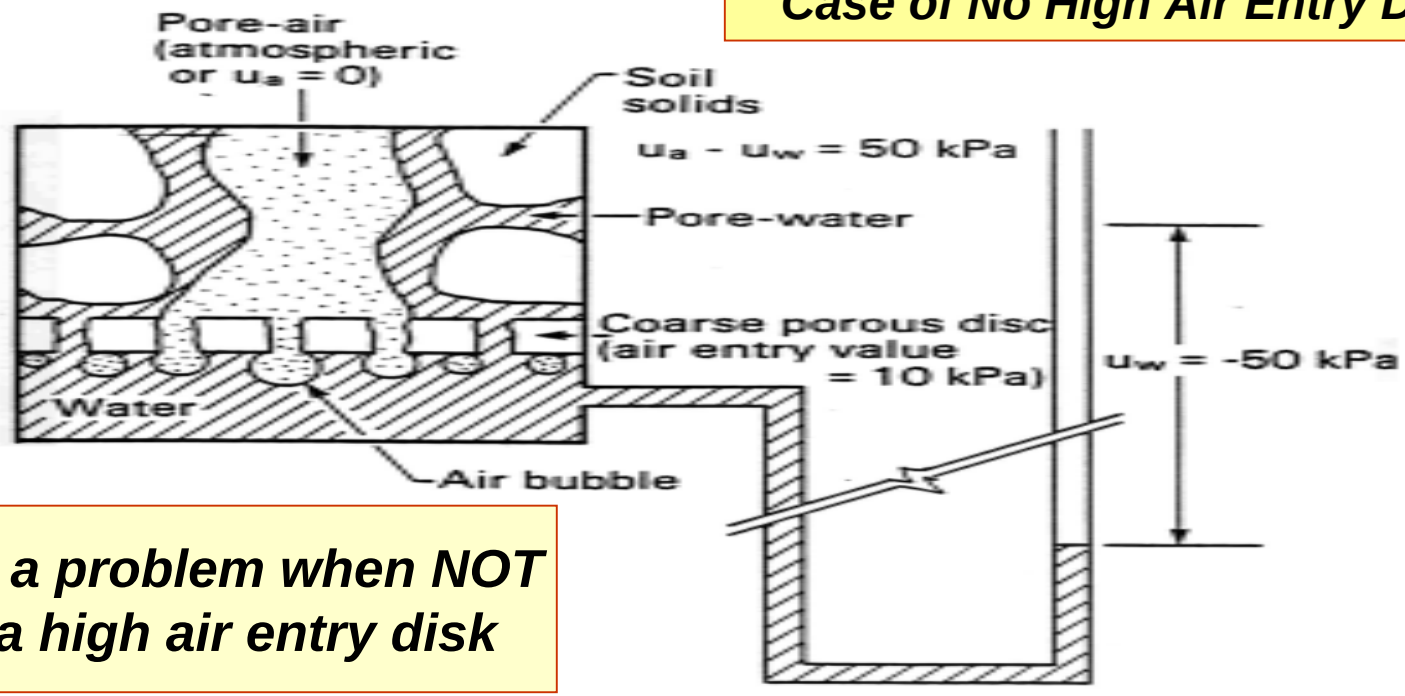

There is a problem when NOT using a high air entry disk

(a) Air intrusion through porous disk when its air entry value is exceeded

Direct measurement of pore-water pressure in an unsaturated soil specimen (not to scale)

Axis-Translation Technique

Case of Negative Pore-water Pressures less than -100 kPa with a High Air Entry Disk

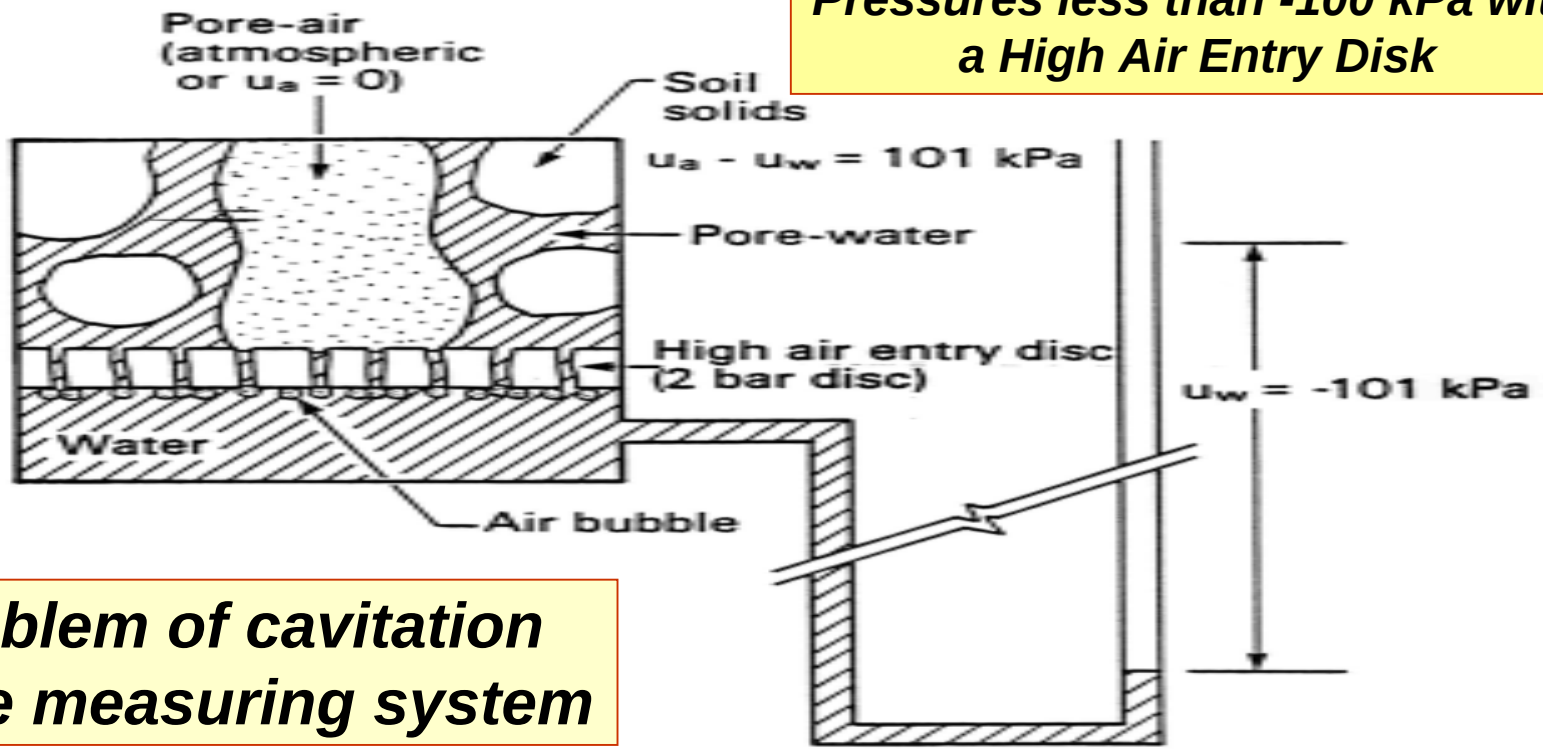

Problem of cavitation In the measuring system

(b) Water cavitation in the measuring system

Direct measurement of pore-water pressure in an unsaturated soil specimen (not to scale)

Axis-Translation Technique

Case of High Air Entry Disk and Axis-translation

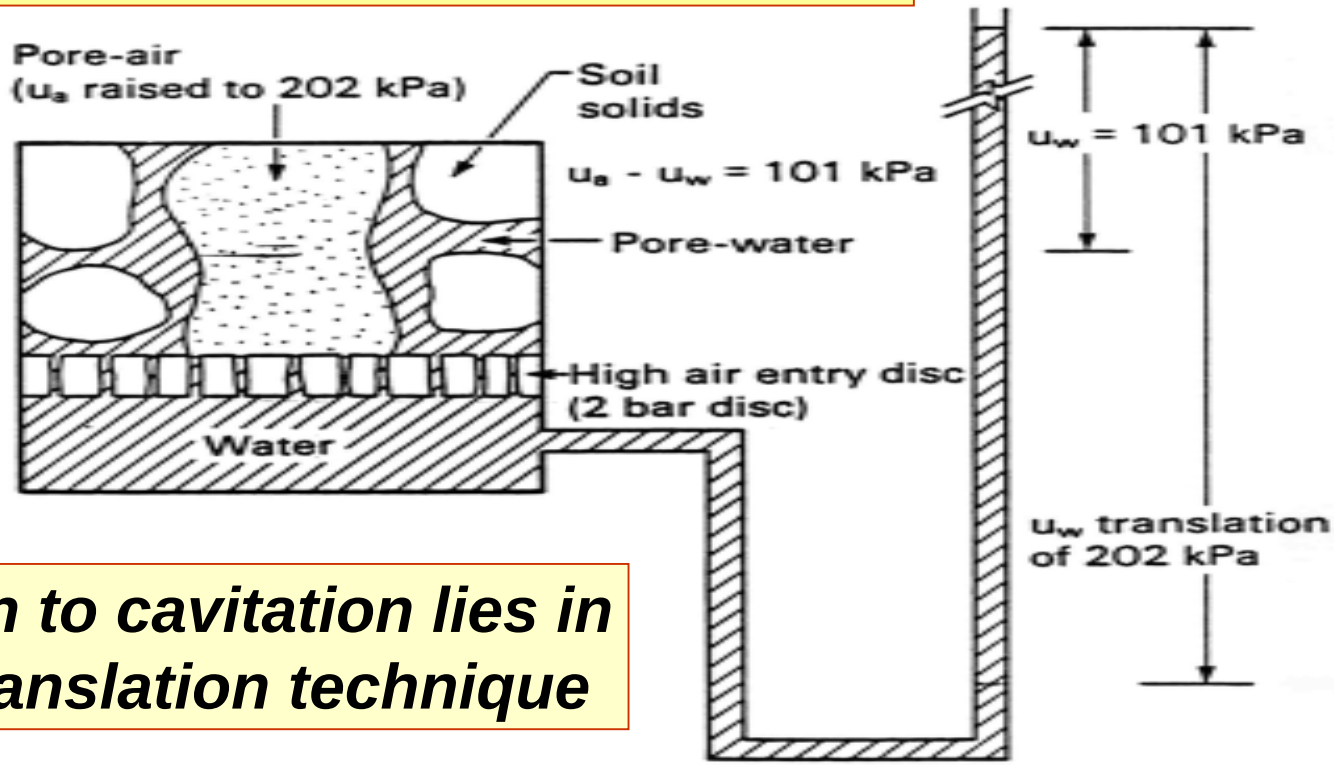

Solution to cavitation lies in Axis-translation technique

(a) Axis-translation of 101 kPa

Measurements of pore-water pressure in an unsaturated soil specimen using the axis-translation technique (not to scale)

Axis-Translation Technique

Case of High Air Entry Disk and Axis-translation

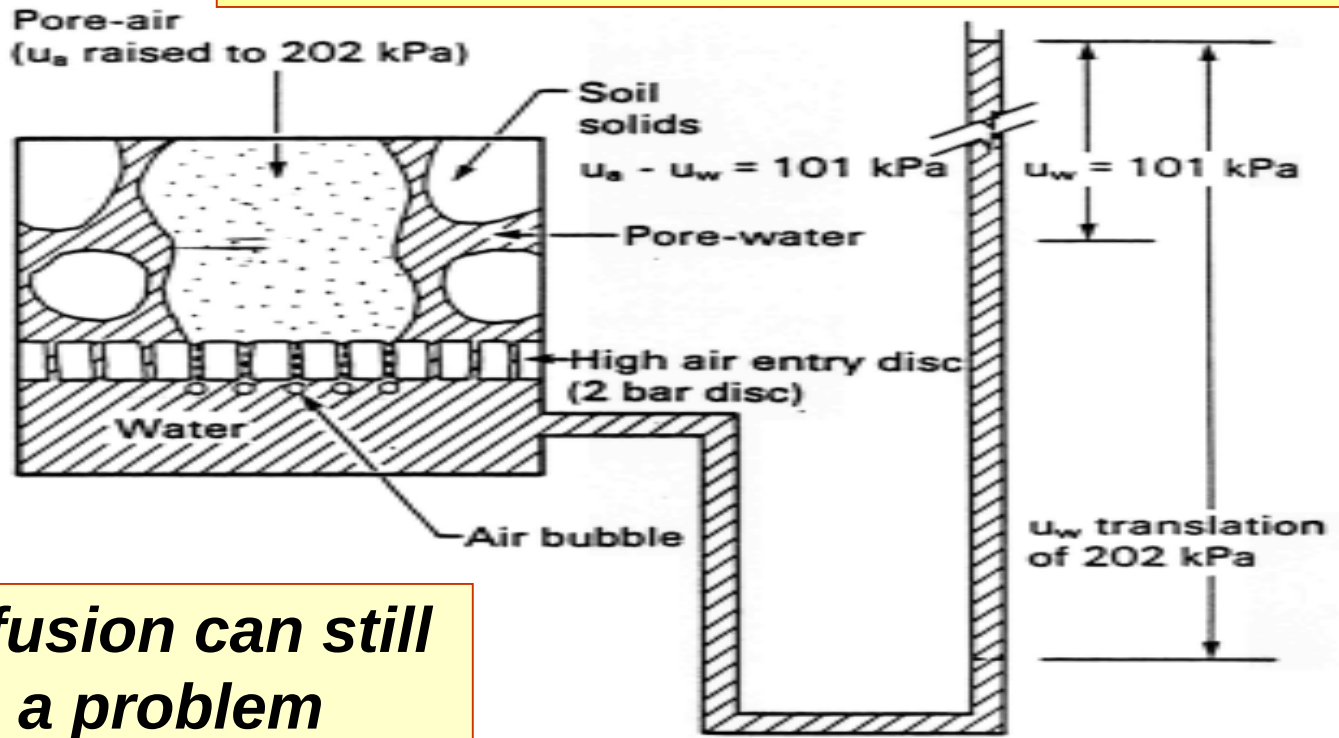

Air diffusion can still be a problem

(b) Air diffusion through the high air entry disk

Measurements of pore-water pressure in an unsaturated soil specimen using the axis-translation technique (not to scale)

Does axis-Translation really work?

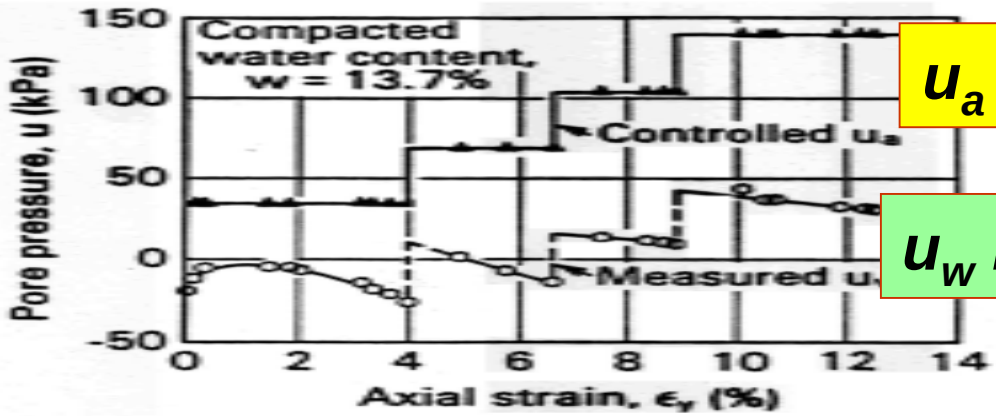

u_a controlled

u_w measured

(a) Pore pressures versus axial strain curve

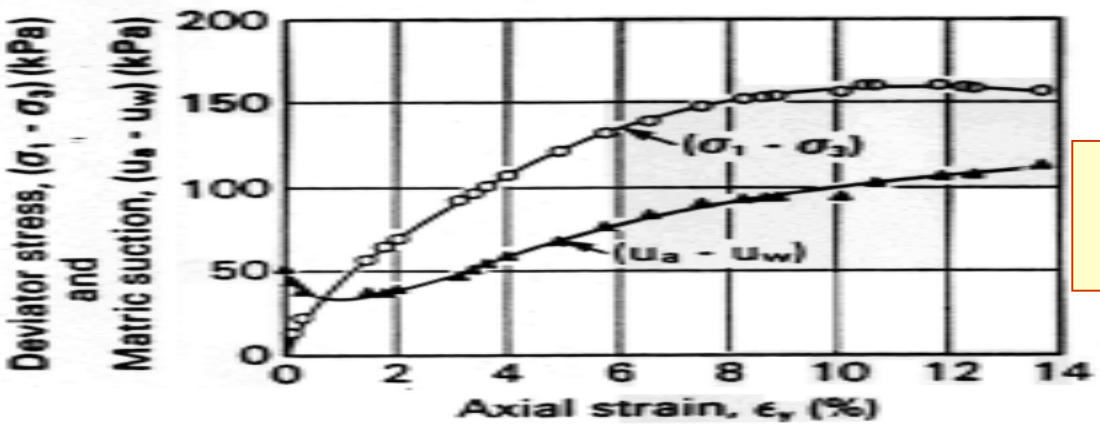

Suction = 110 kPa

(b) Deviator stress and matric suction versus axial strain curves

"Unconfined triaxial" test on a compacted Selset clay specimen at various pore-air pressures (from Bishop and Blight, 1963)

Does axis-Translation really work?

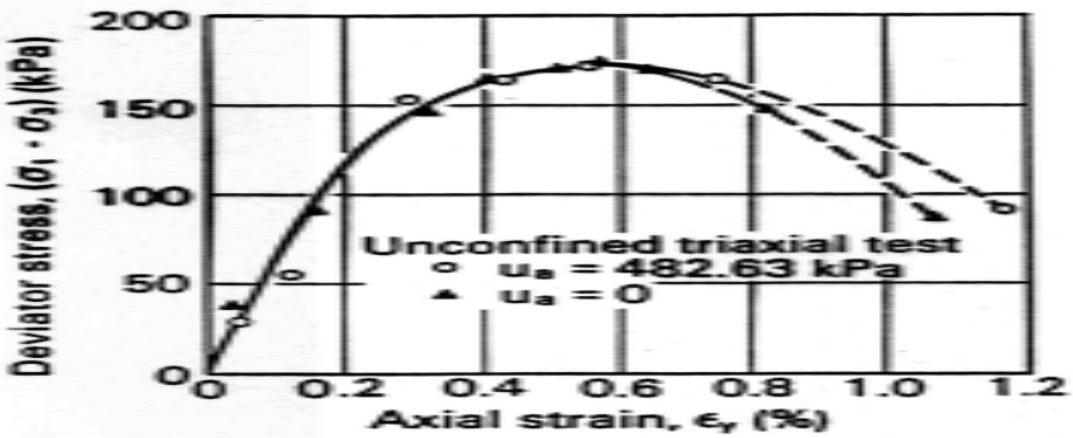

(a) Deviator stress versus axial strain curve

u_a = 483 kPa; u_w = 69 kPa (Suction = 414 kPa)

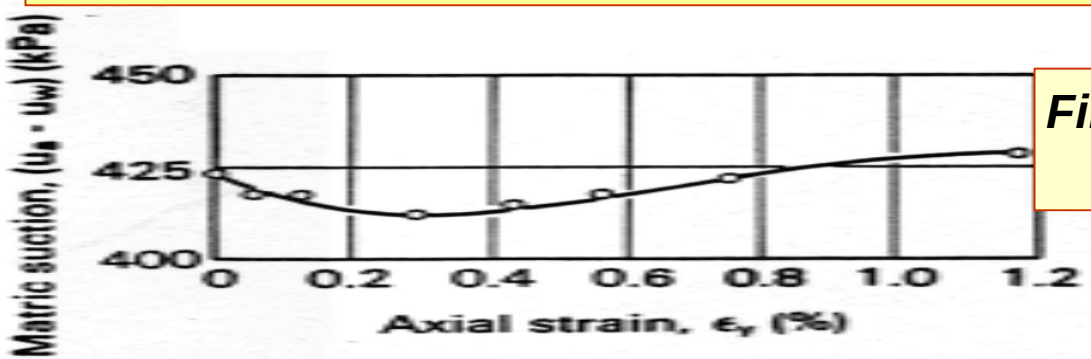

Final Suction = 430 kPa

(b) Matric suction versus axial strain during the test with axis-translation

"Unconfined triaxial" tests on a compacted Talybont clay with and without axis-translation (from Bishop and Blight, 1963)

High Air Entry Disks at Imperial College (From Blight, 1961)

Type	Porosity, n (%)	Coefficient of Permeability, k_d (m/s)	Air Entry Value, $(u_a - u_w)$ (kPa)
Doulton Grade P6A	23	2.1×10^{-9}	152
Aerox "Celloton" Grade VI	46	2.9×10^{-8}	214
aolin-consolidated from a slurry and fired	45	6.2×10^{-10}	317
Kaolin-dust pressed and fired	39	4.5×10^{-10}	524

High Air Entry Disks Manufactured by Soilmoisture Equipment Corporation

Type	Approximate Pore Diameter ($\times 10^{-3}$ mm)	Coefficient of Permeability, k_d (m/s)	Air Entry Value Range, $(u_a - u_w)$ (kPa)
1/2 bar (high flow)	6.0	3.11×10^{-7}	48–62
1 bar	2.1	3.46×10^{-9}	138–207
1 bar (high flow)	2.5	8.6×10^{-8}	131–193
2 bar	1.2	1.73×10^{-9}	241–310
3 bar	0.8	1.73×10^{-9}	317–483
5 bar	0.5	1.21×10^{-9}	>550
15 bar	0.16	2.59×10^{-11}	>1520

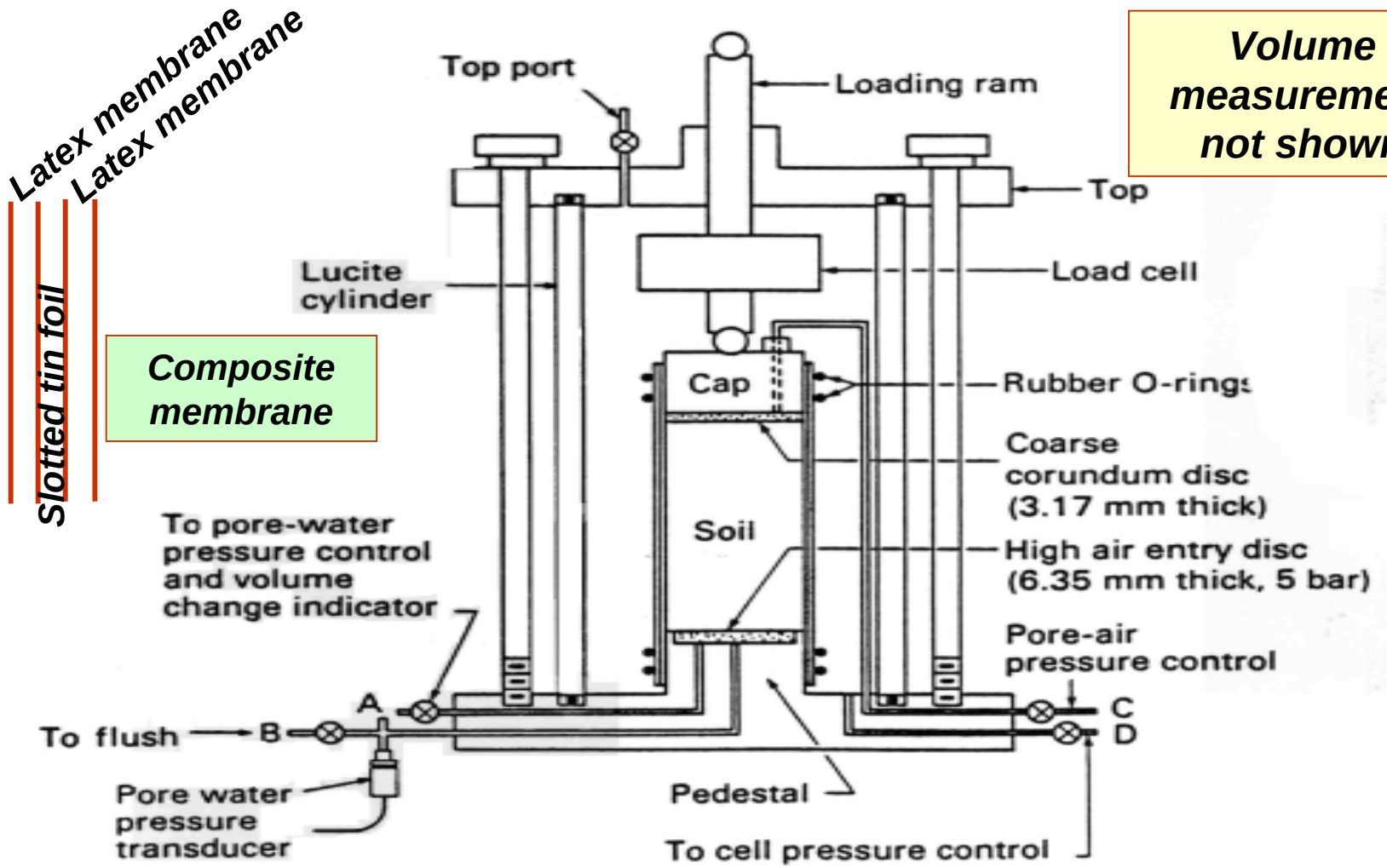

Modified triaxial cell for testing unsaturated soils

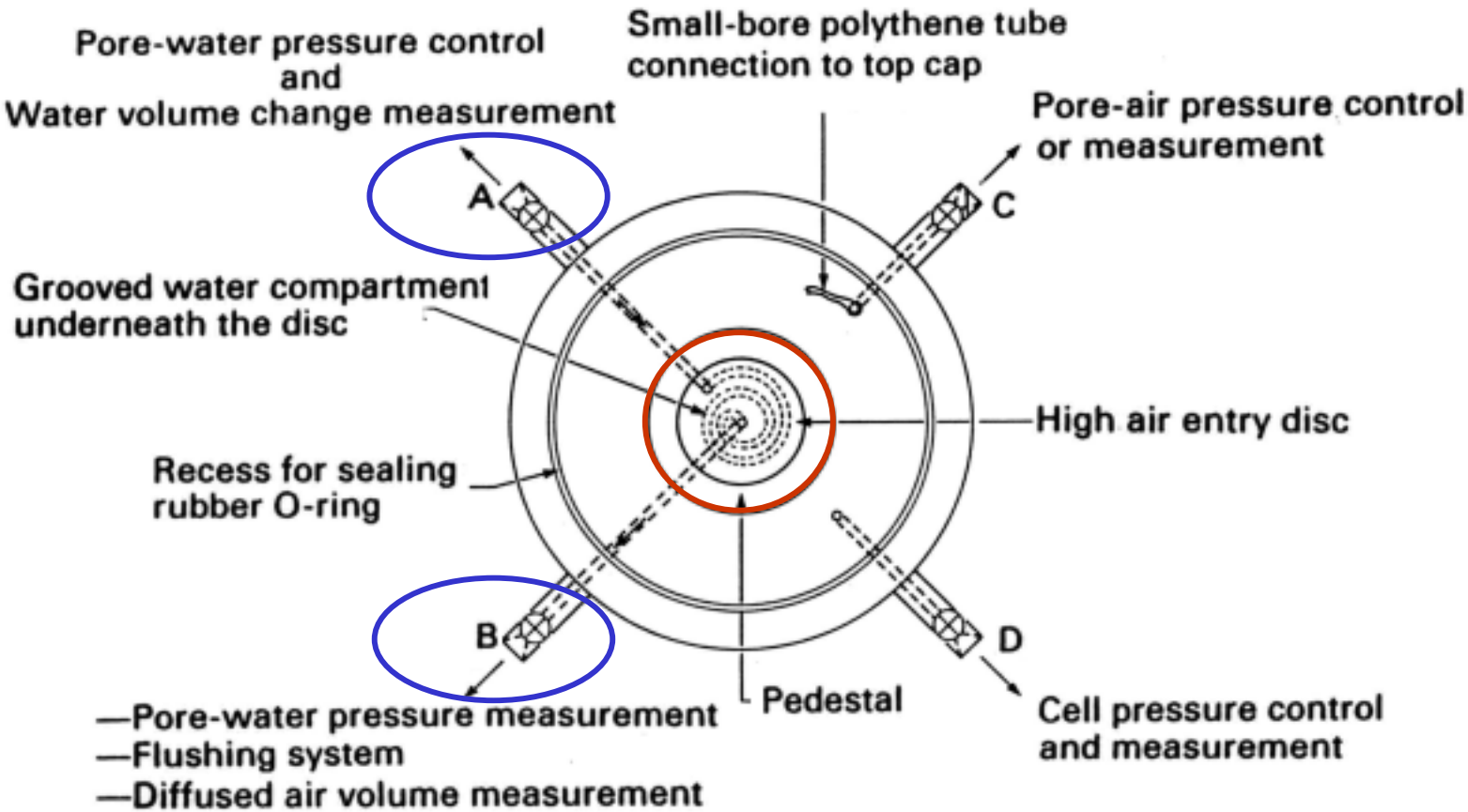

(a) Plan view of the base plate with its outlet ports

Triaxial base plate for unsaturated soil testing

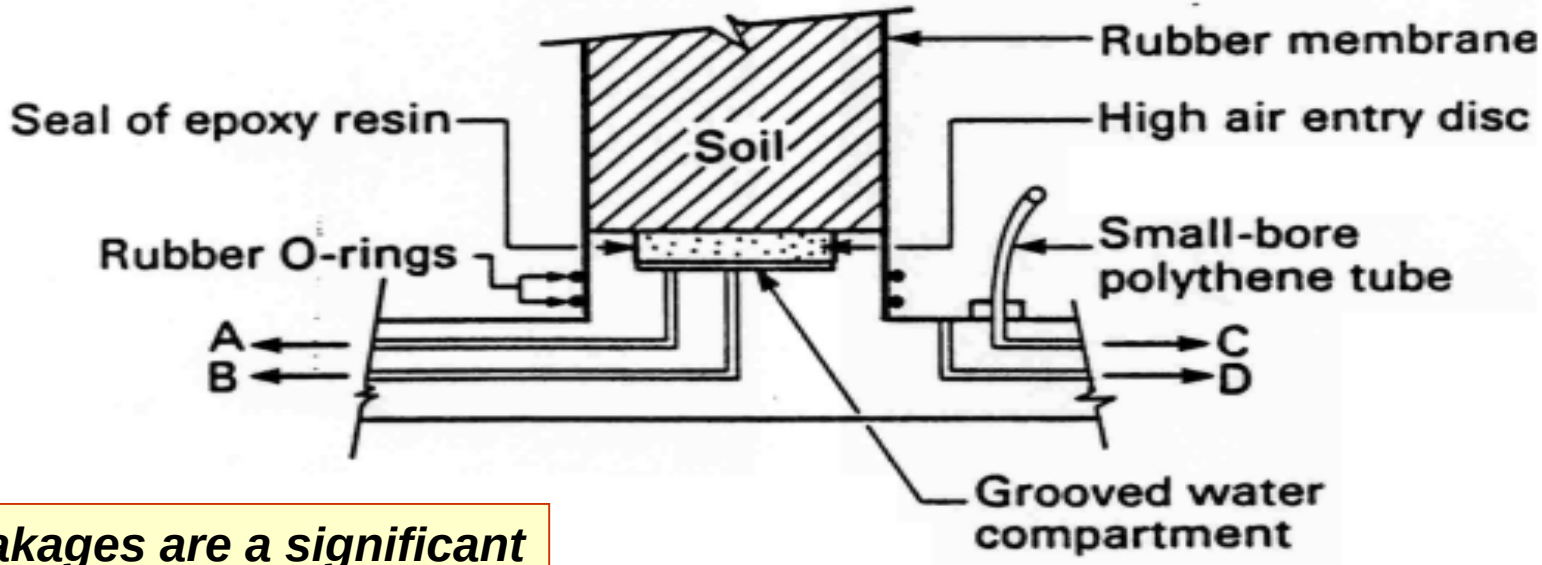

Leakages are a significant problem in unsaturated soil testing

(b) Cross-section of a base plate with a high air entry disk

Triaxial base plate for unsaturated soil testing

Modified direct shear equipment for testing an unsaturated soil specimen (from Gan, 1986)

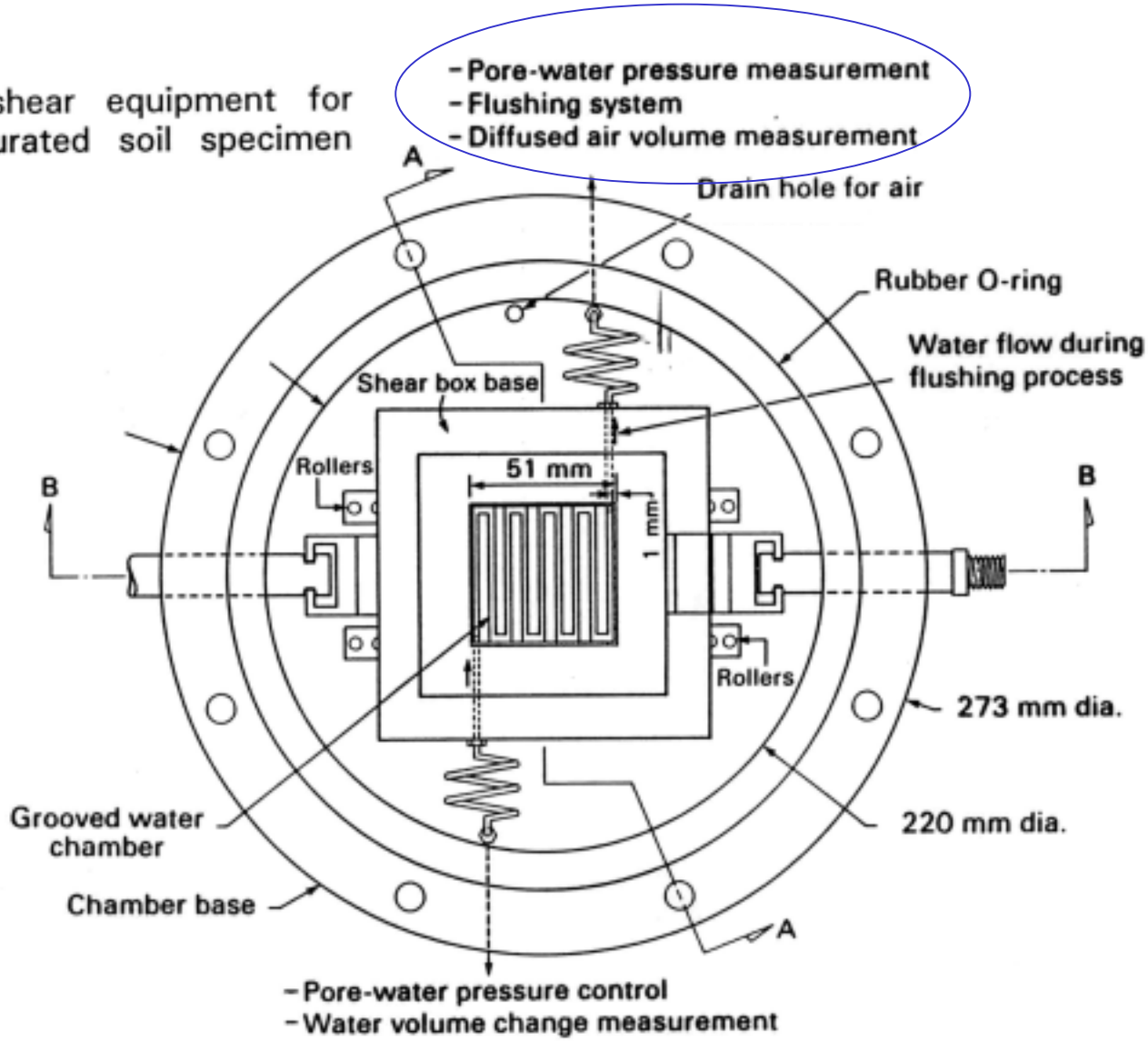

(a) Plan view of the pressure chamber of a direct shear box

Bottom part of shear box must move because of the vertical piston load

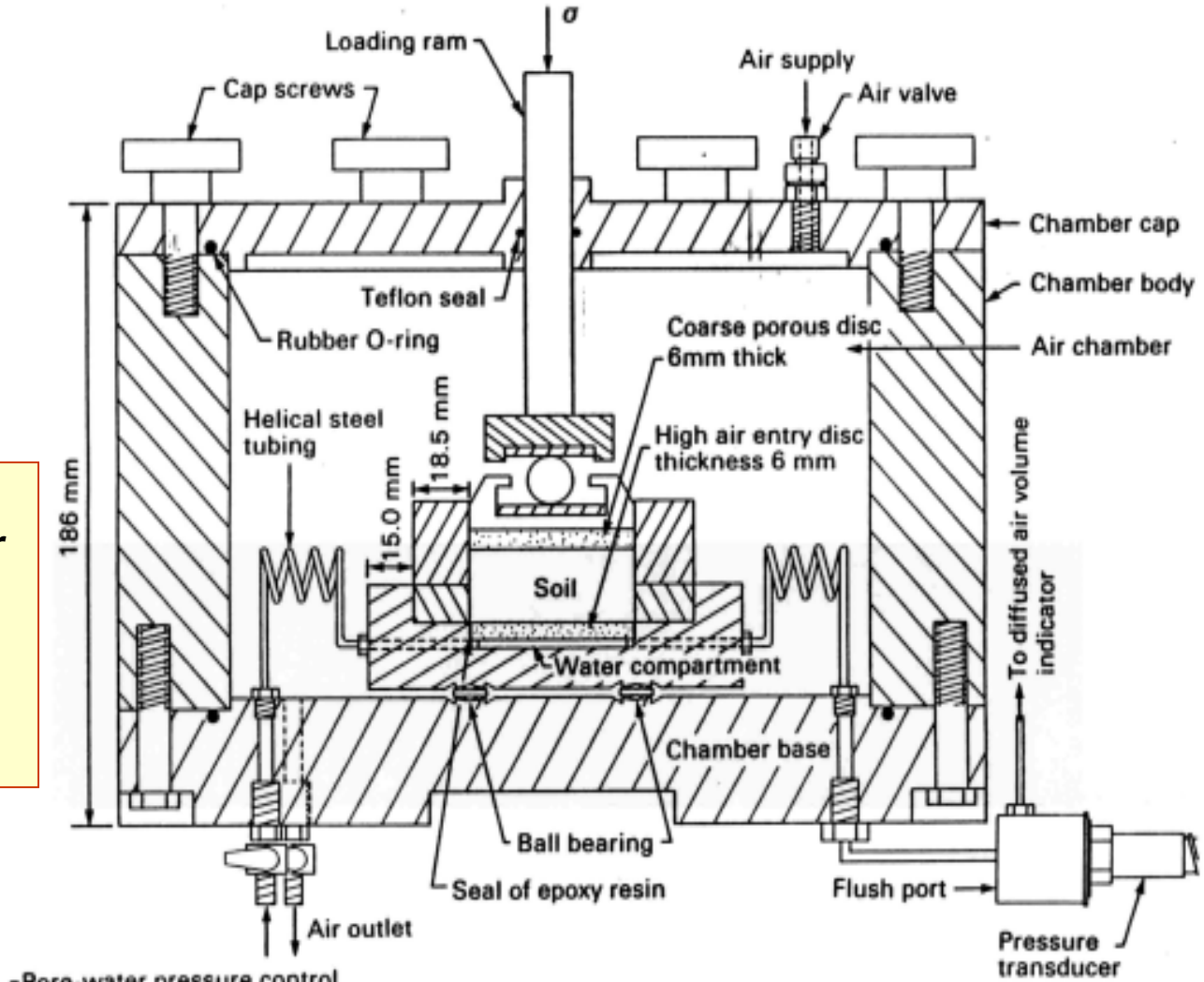

(b) Cross-sectional view A-A of a direct shear box and pressure chamber

Modified direct shear equipment for testing an unsaturated soil specimen (from Gan, 1986)

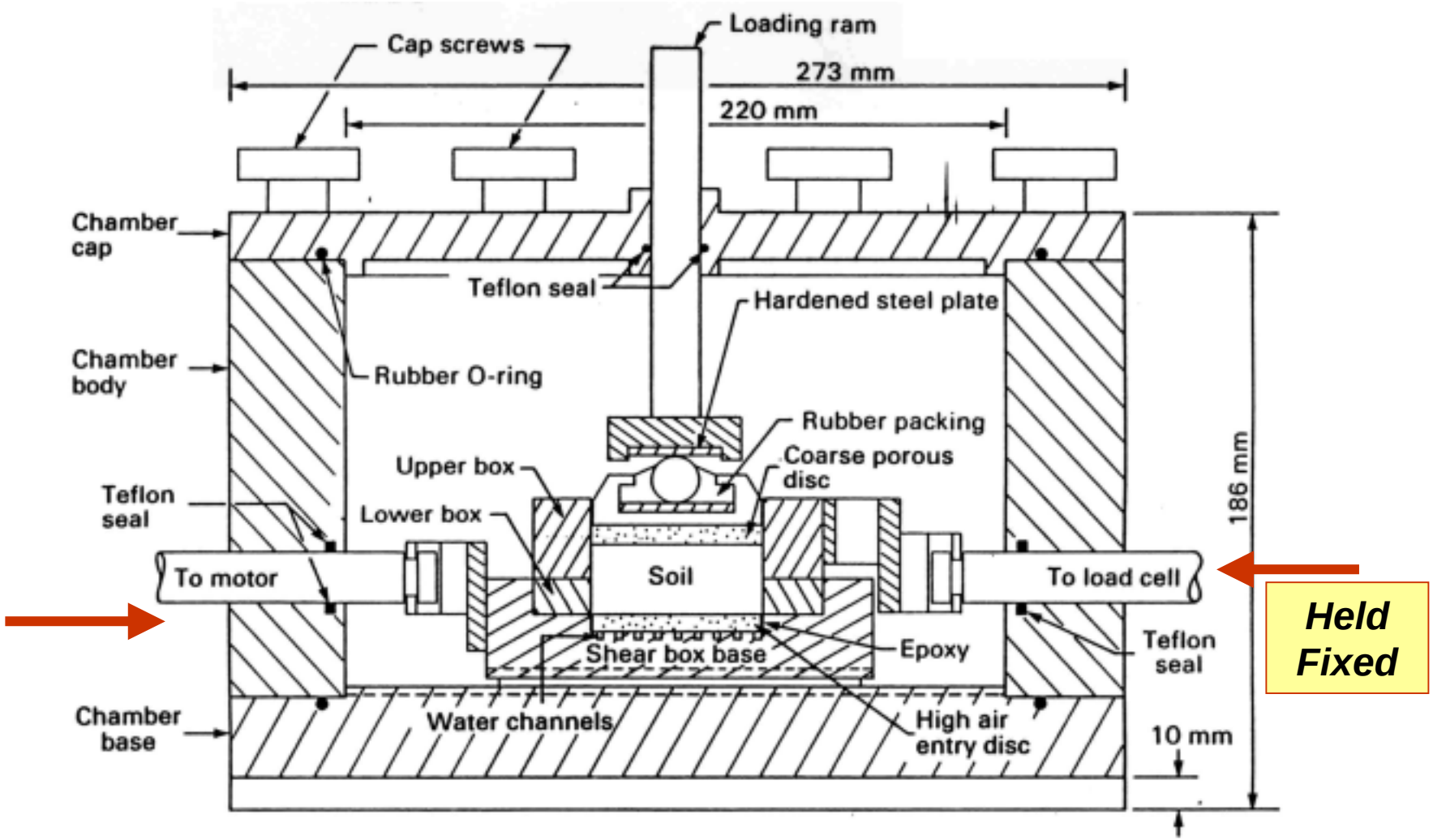

Modified direct shear apparatus for testing unsaturated soils (from Gan and Fredlund, 1988)

Air pressure is usually controlled at the top of the specimen through a coarse disk

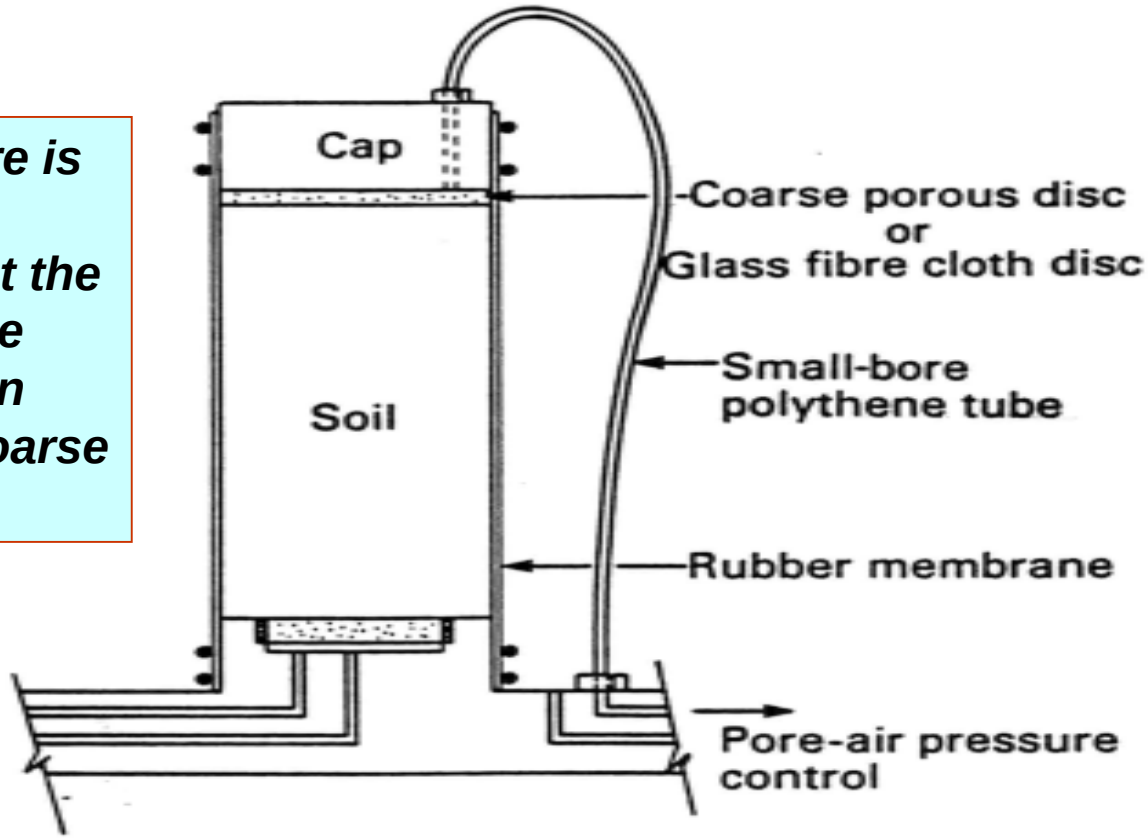

Pore-air pressure control system

Measurement of overall volume change

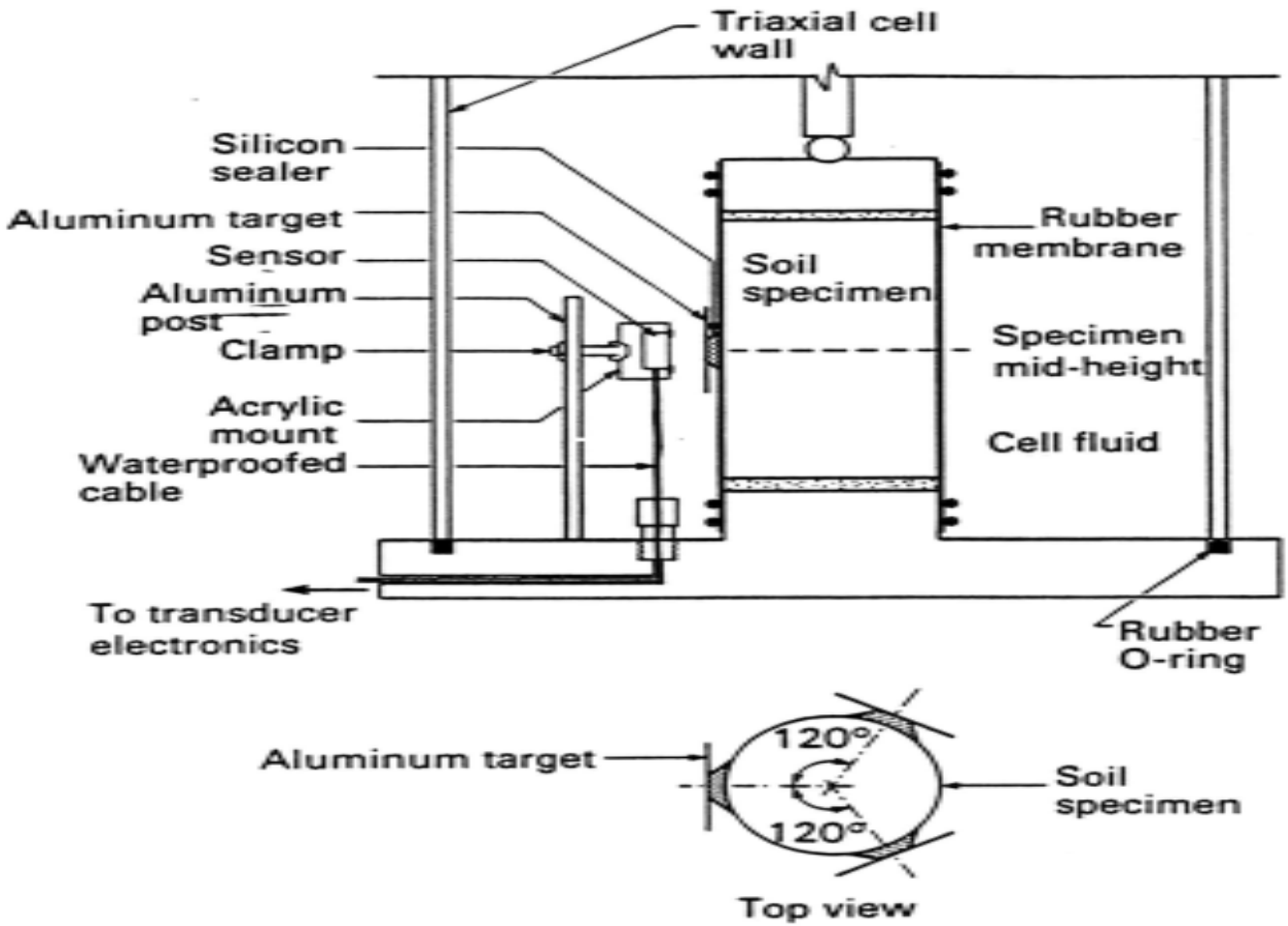

Installation of a non-contacting radial deformation transducer (from Drumright, 1987)

Require three non-contact sensors but still not a perfect solution for overall volume change

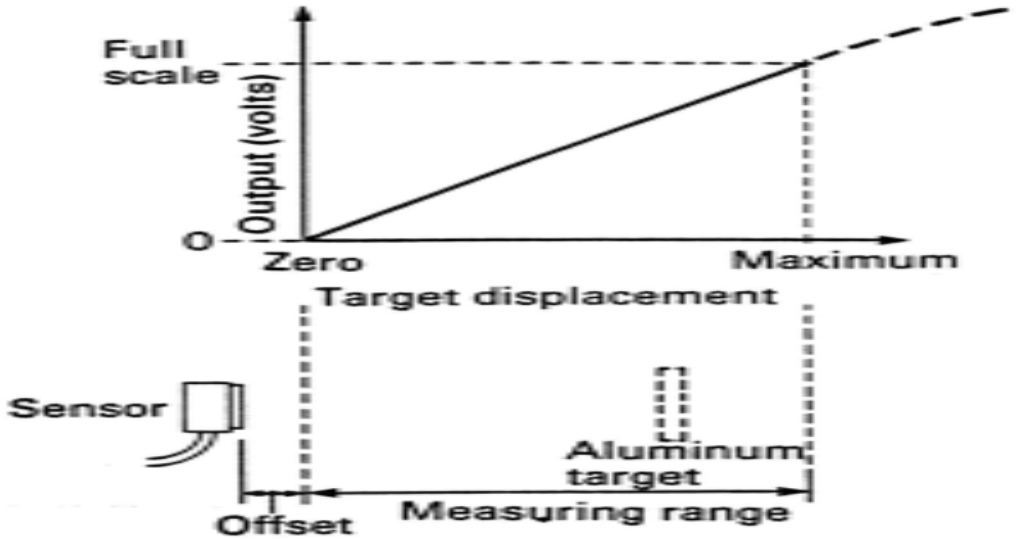

(a) Calibration

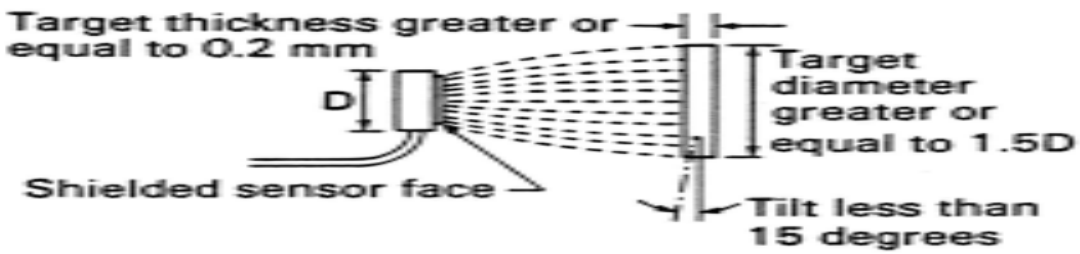

(b) Installation requirements

Non-contacting radial deformation transducer, KD-2310 series, model 4SB, shielded, button-type (from Karman Science Corporation)

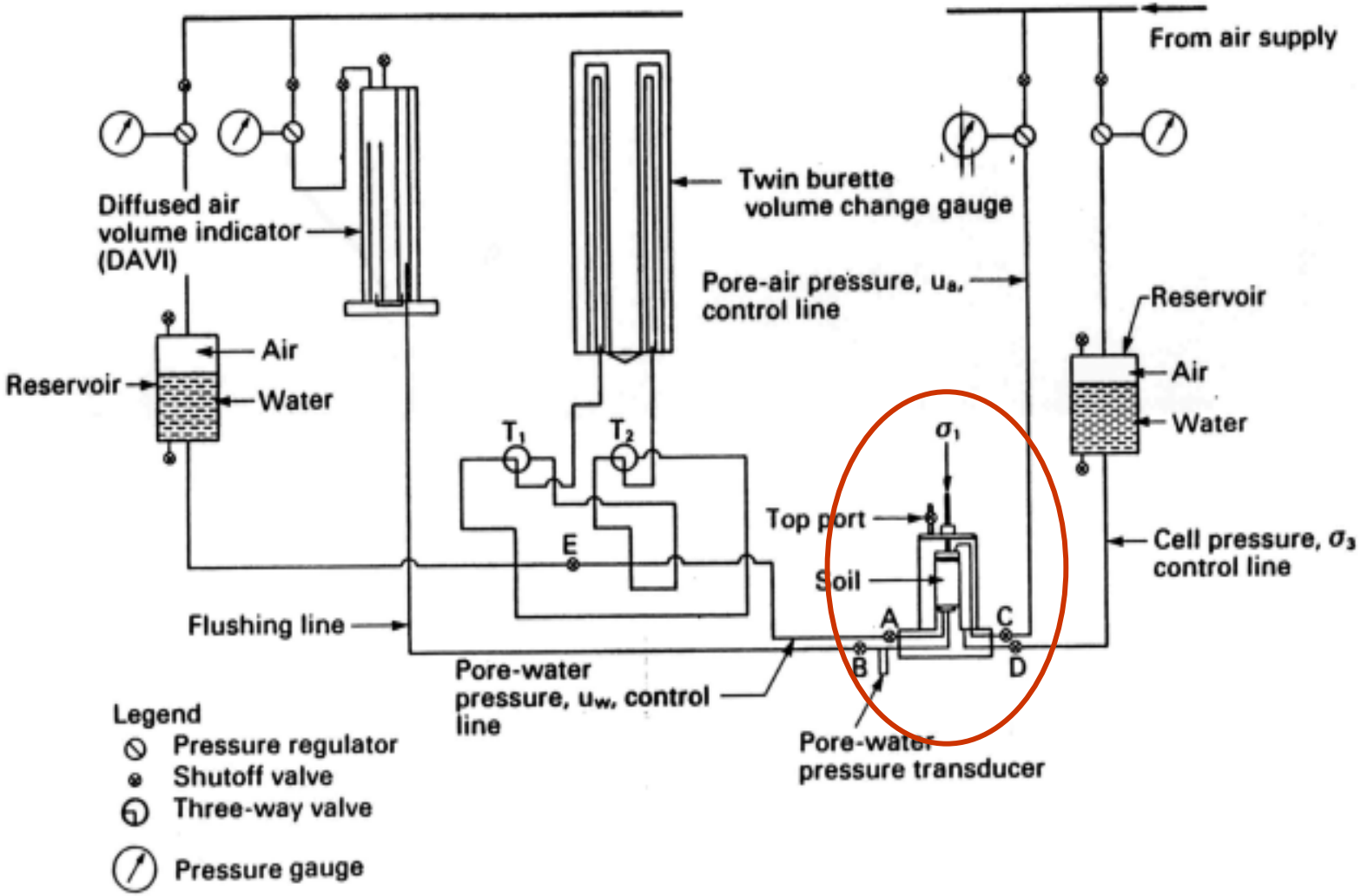

Schematic diagram of the control board and plumbing layout for the modified triaxial apparatus

Typical Multistage Triaxial Test Results on Decomposed Granite

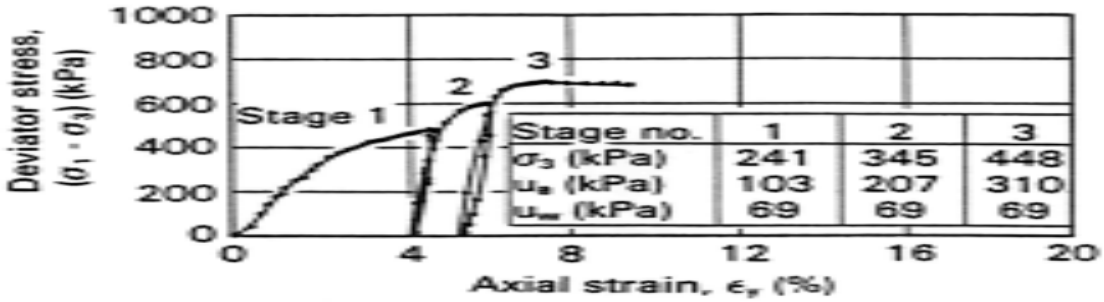

(a) Deviator stress versus strain curve

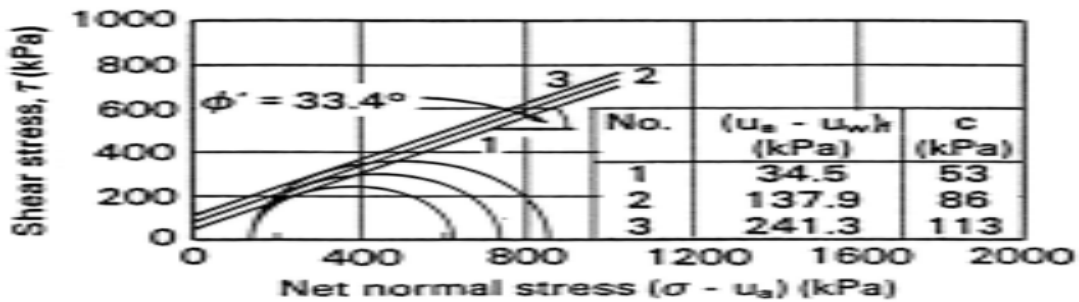

(b) Failure envelope projection onto the τ versus $(\sigma - u_a)$ plane

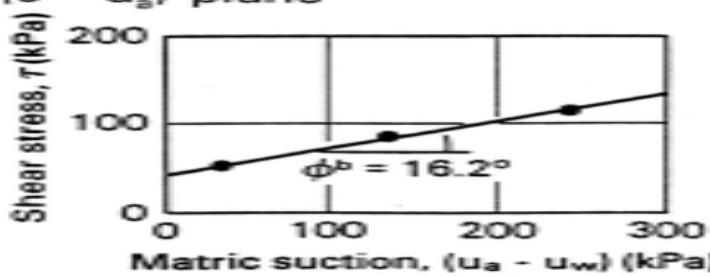

(c) Intersection line between the failure envelope and the τ versus $(u_a - u_w)$ plane

Stress versus strain curves and two-dimensional presentations of the failure envelope for decomposed granite specimen no. 10 (from Ho and Fredlund 1982a)

Typical Multistage Triaxial Test Results on Silt

Specimen E-3

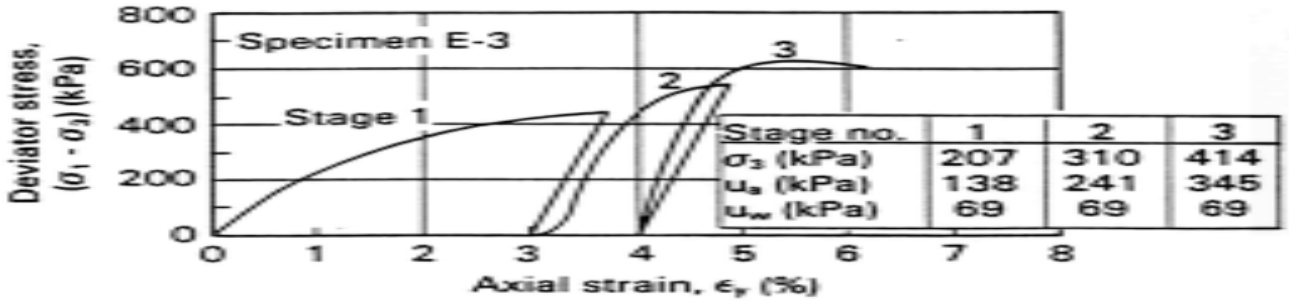

(a) Deviator stress versus strain curve

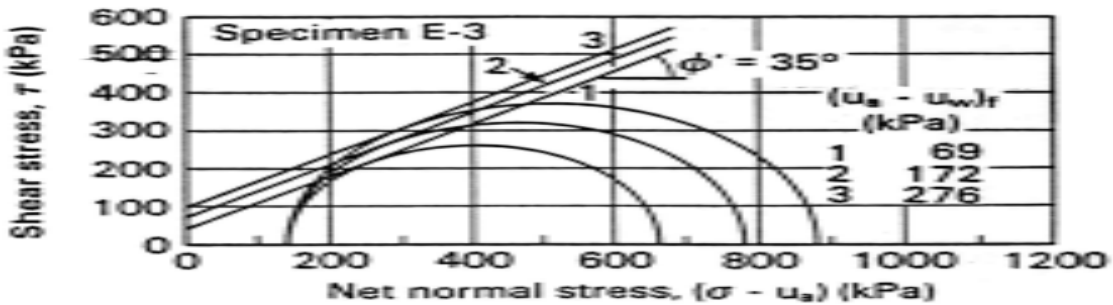

(b) Failure envelope projection onto the τ versus $(\sigma - u_a)$ plane

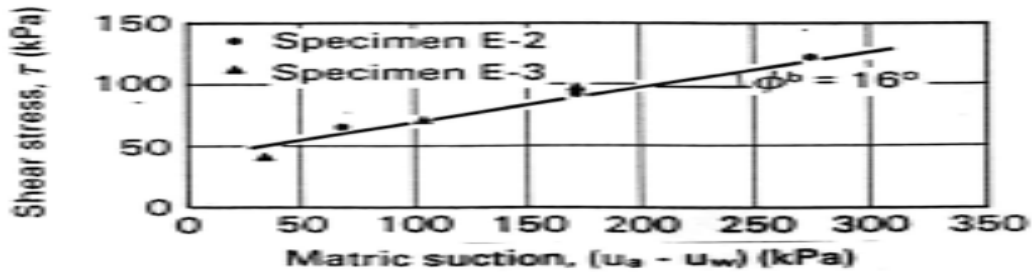

(c) Intersection line between the failure envelope and the τ versus $(u_a - u_w)$ plane

Stress versus strain curves and two-dimensional presentations of the failure envelope for Tappen-Notch Hill Silt specimen no. E-3 (from Krahn, Fredlund and Klassen, 1987)

Increase in strength with matric suction

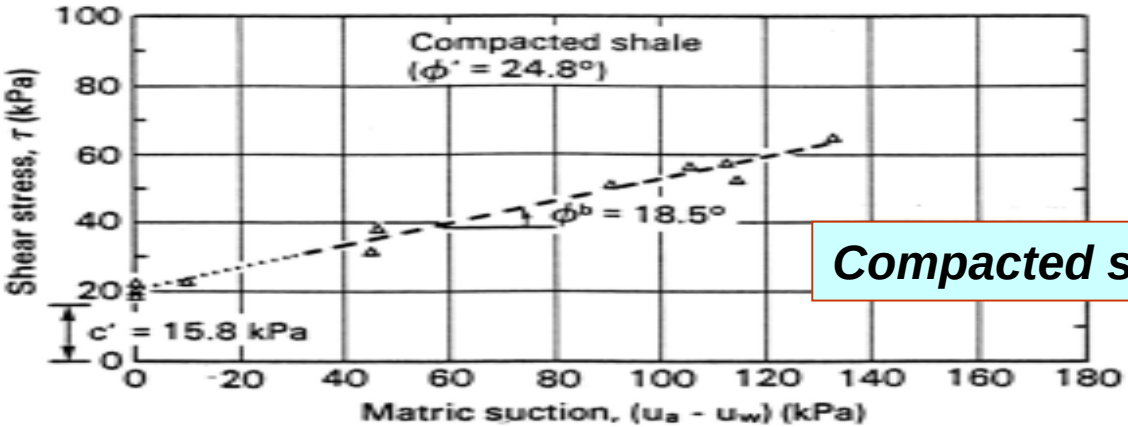

Compacted shale

Intersection line between the failure envelope and the τ versus (u_a - u_w) plane or a compacted shale (data from Bishop, Alpan, Blight and Donald, 1960)

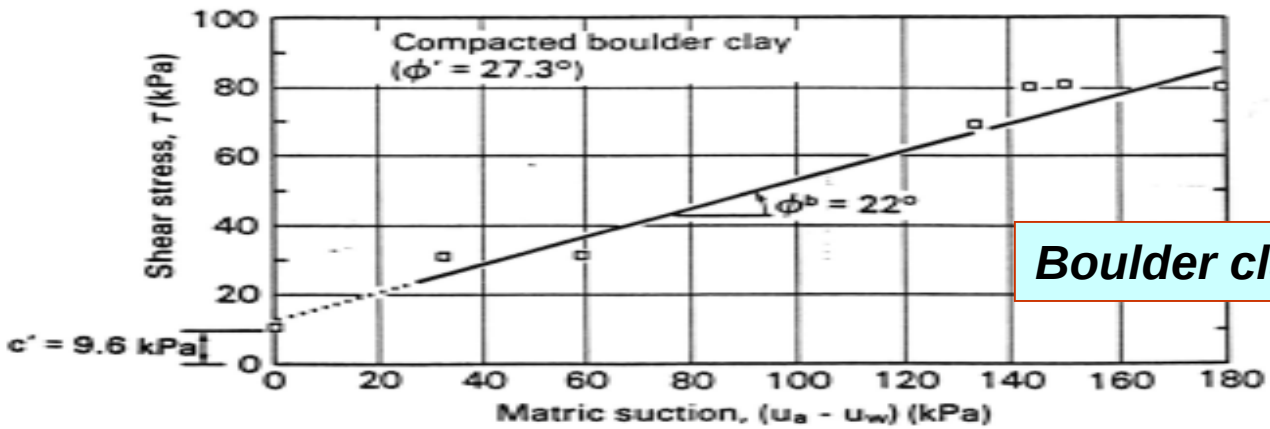

Boulder clay

Intersection line between the failure envelope and the τ versus (u_a - u_w) plane for a compacted boulder clay (data from Bishop, Alpan, Blight and Donald, 1960)

Increase in strength with matric suction for Dhanauri clay compacted at a low density

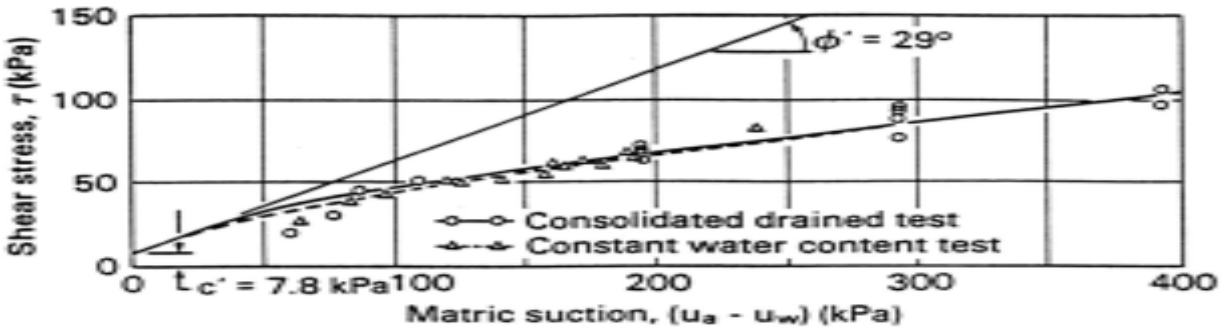

(a) Curved failure envelopes for Dhanauri clay compacted to a low density

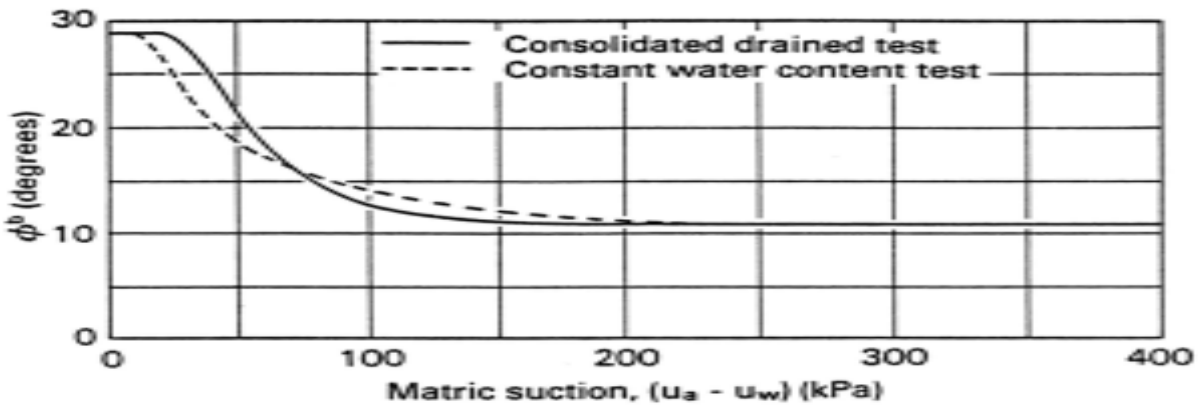

(b) Nonlinear relationship between ϕ^b and matric suction

Nonlinearity in the failure envelope with respect to matric suction for Dhanauri clay compacted to a low density

Increase in strength with matric suction for Dhanauri clay compacted at a high density

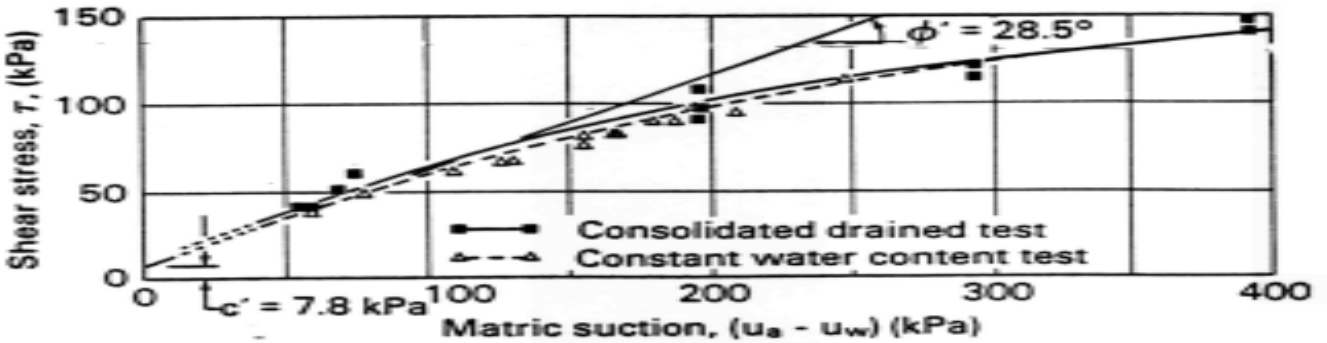

(a) Curved failure envelopes for Dhanauri clay compacted to a high density (data from Satija, 1978)

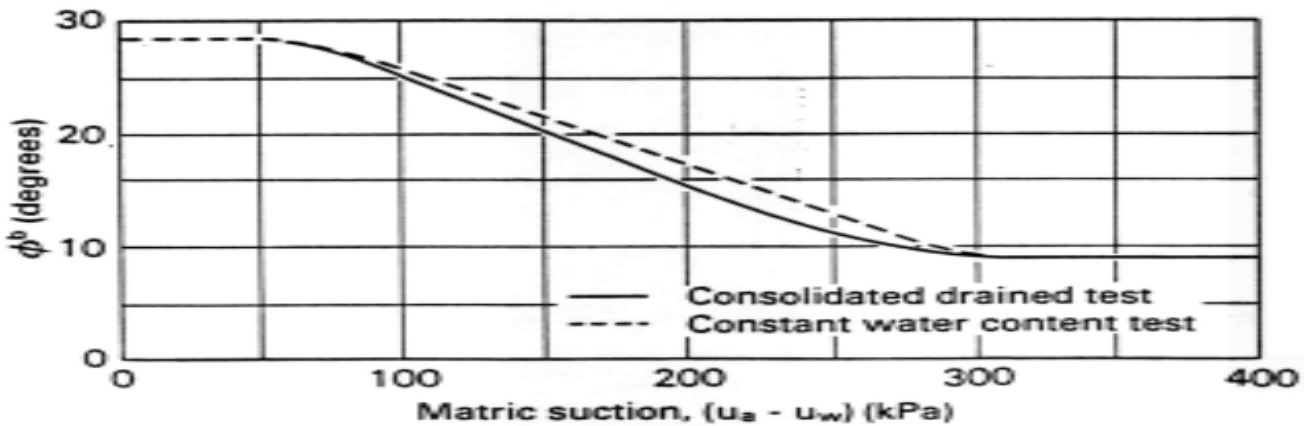

(b) Nonlinear relationship between ϕ^b and matric suction

Nonlinearity in the failure envelope with respect to matric suction for Dhanauri clay compacted to a high density

Results of a series of confined and unconfined compression tests on a compacted clayey sand compacted to a high density

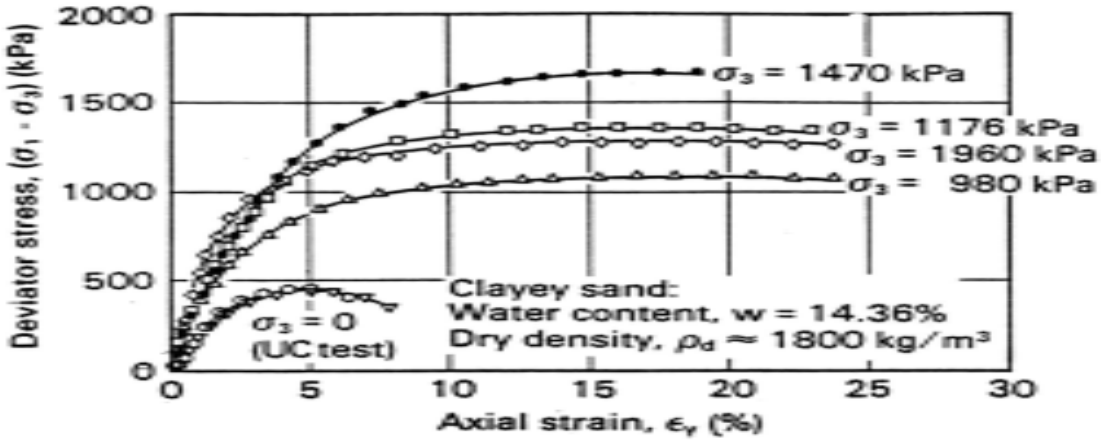

(a) Deviator stress versus strain for various confining pressures

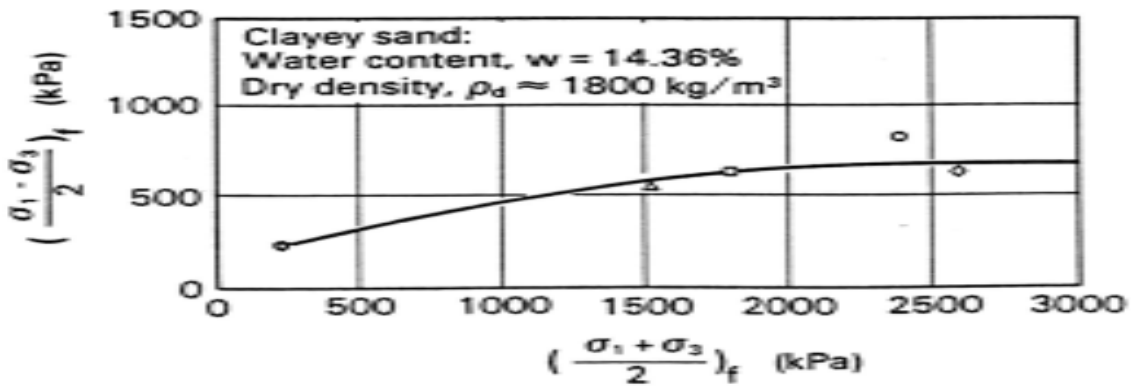

(b) Total stress point envelope

Undrained triaxial and unconfined compression tests on a clayey sand compacted to a high density (from Chantawarangul, 1983)

Results of a series of confined and unconfined compression tests on a compacted clayey sand compacted to a low density

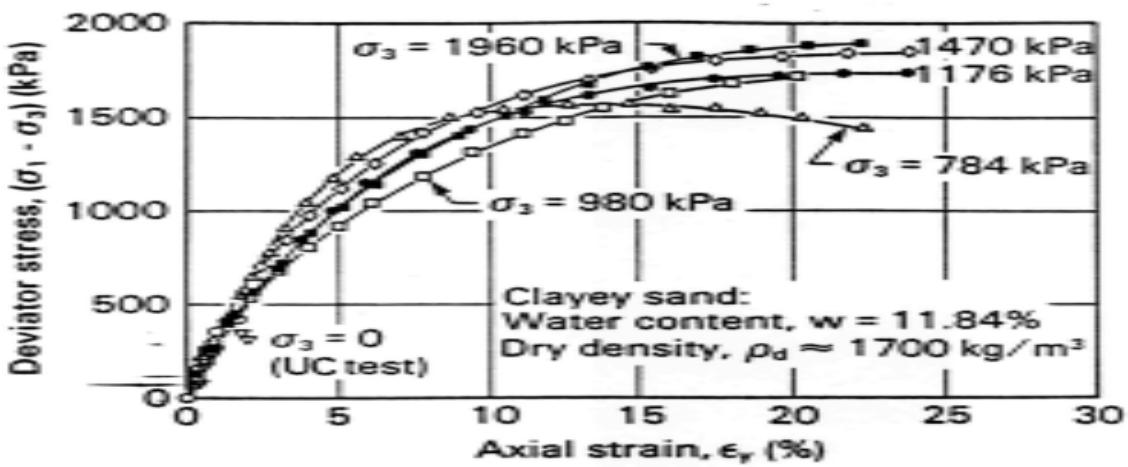

(a) Deviator stress versus strain for various confining pressures

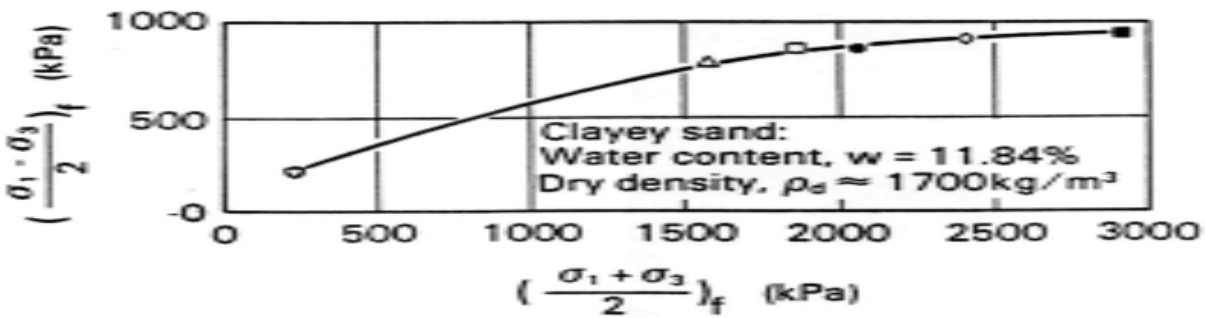

(b) Total stress point envelope

Undrained triaxial and unconfined compression tests on a clayey sand compacted to a low density (from Chantawarangul, 1983)

Effect of confinement on the undrained compressive strength

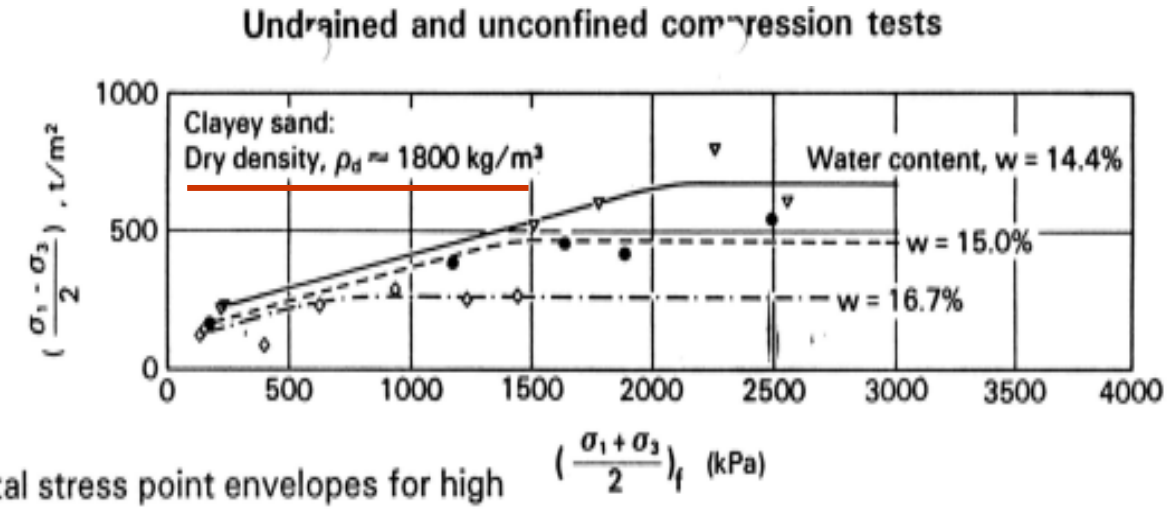

(a) Total stress point envelopes for high density specimens

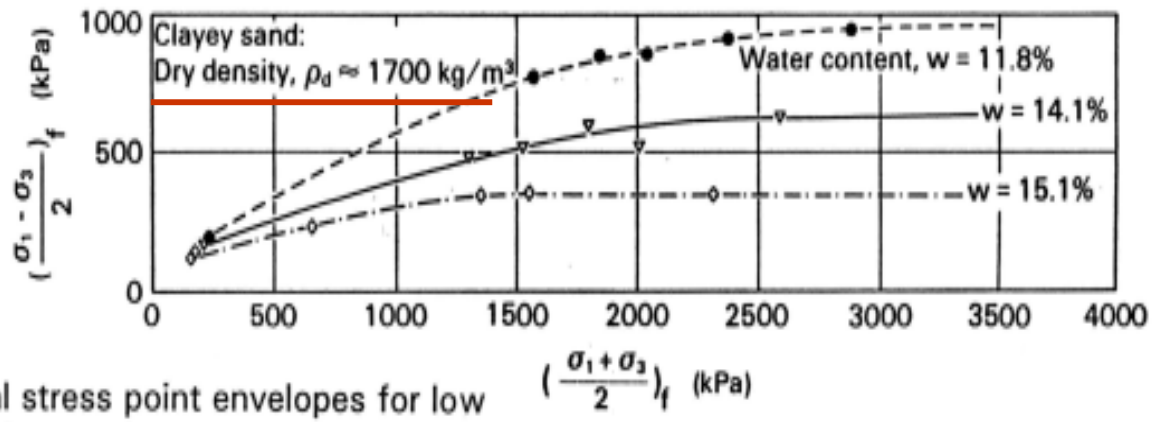

(b) Total stress point envelopes for low density specimens

Total stress point envelopes obtained from undrained triaxial and unconfined compression tests (from Chantawarangul, 1983)

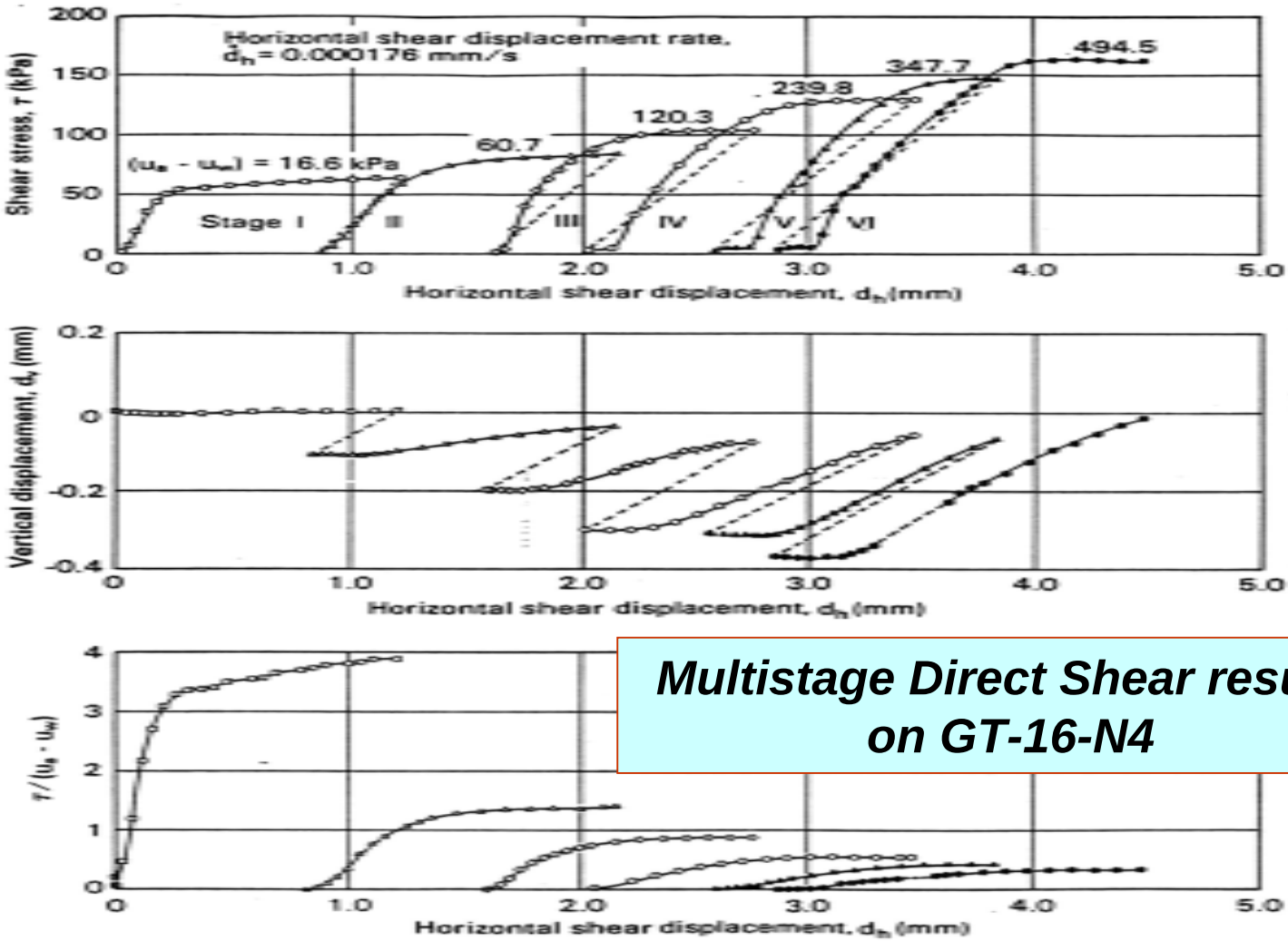

Multistage Direct Shear results on GT-16-N4

Multistage direct shear test results on unsaturated glacial till specimen no. GT-16-N4 (from Gan, Fredlund and Rahardjo, 1987)

Multistage Direct Shear results on GT-16-N4

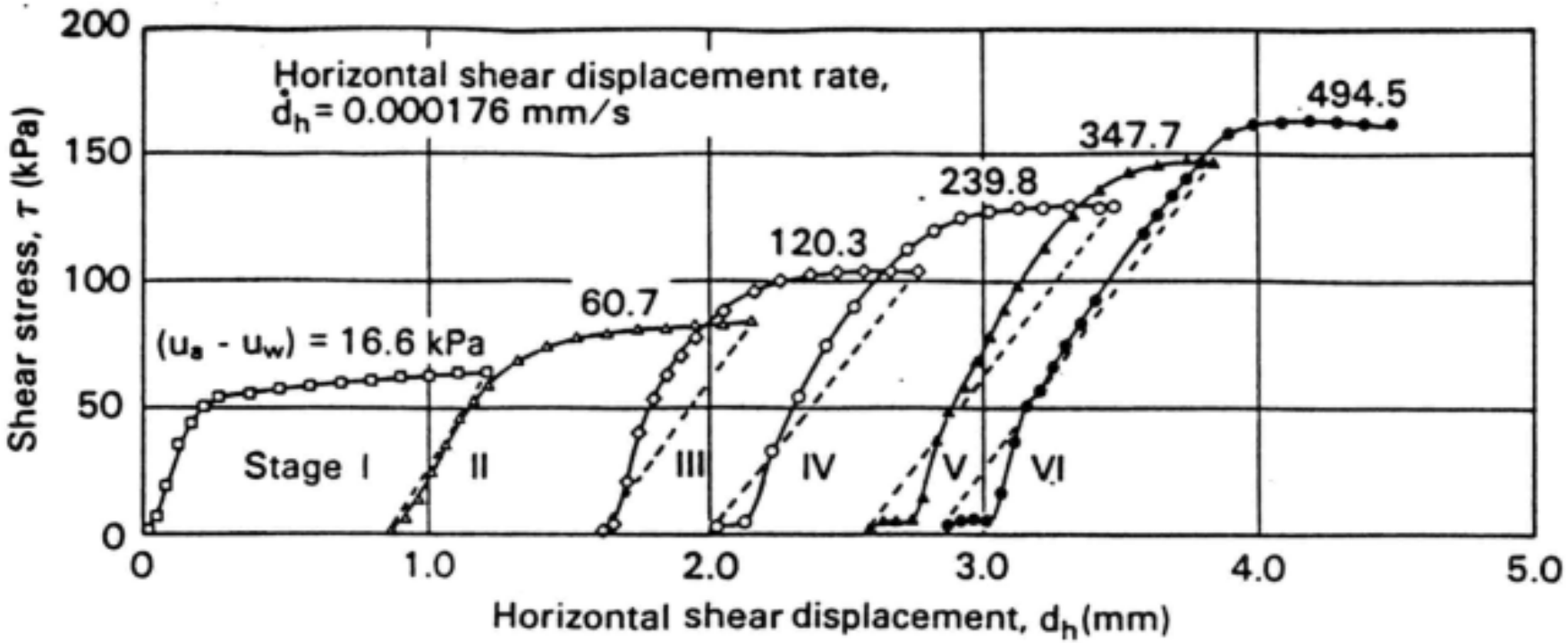

Note the continual increase in strength with an increase in applied matric suction

Nonlinear shear strength versus matric suction

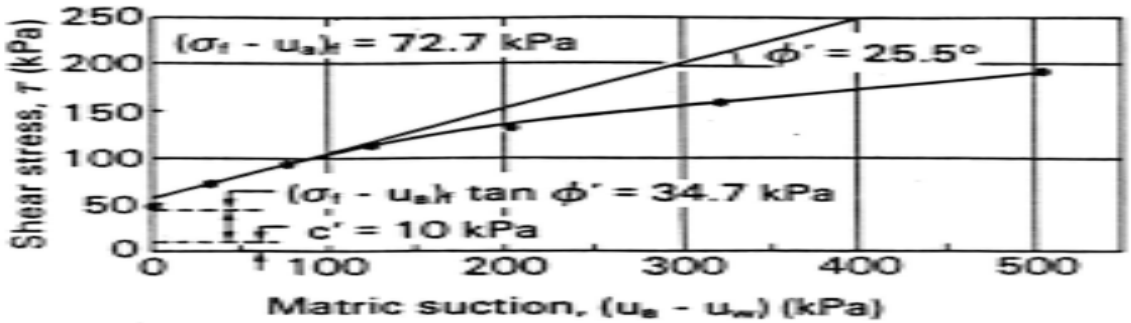

(a) Failure envelope on the τ versus $(u_a - u_w)$ plane

Interpretation for ϕ^b on GT-16-N5

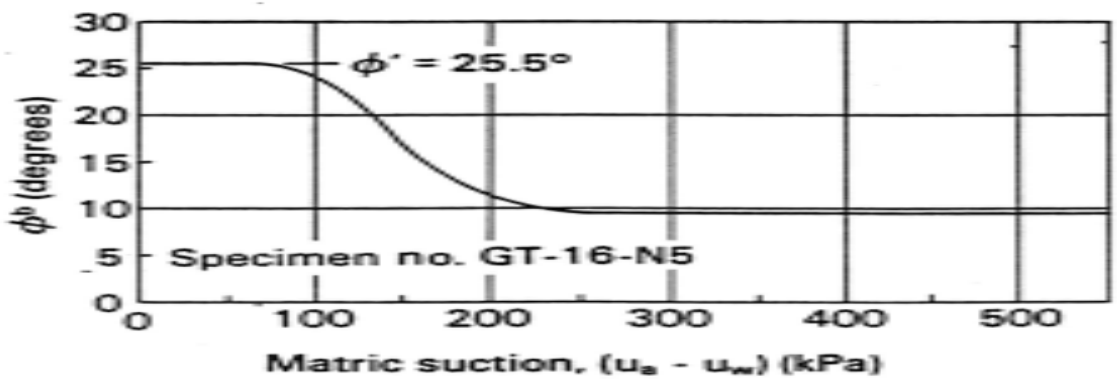

(b) Relationship between the ϕ^b values and matric suction

Failure envelope obtained from unsaturated glacial till specimen no. GT-16-N5 (from Gan and Fredlund, 1988)

Results of a series of Direct Shear tests on glacial till

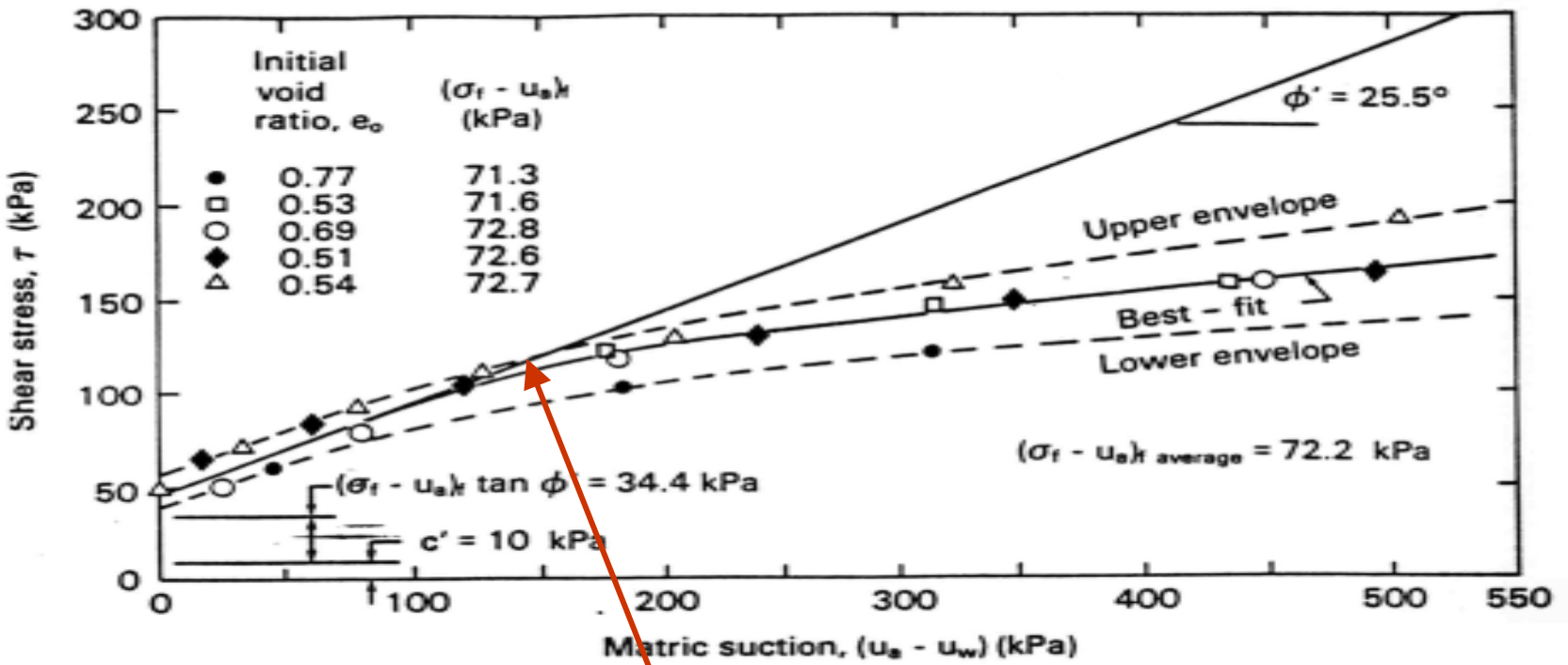

(a) Failure envelopes on the τ versus $(u_a - u_w)$ plane

Commencement of desaturation of the soil

Linear on the Net Normal Stress plane

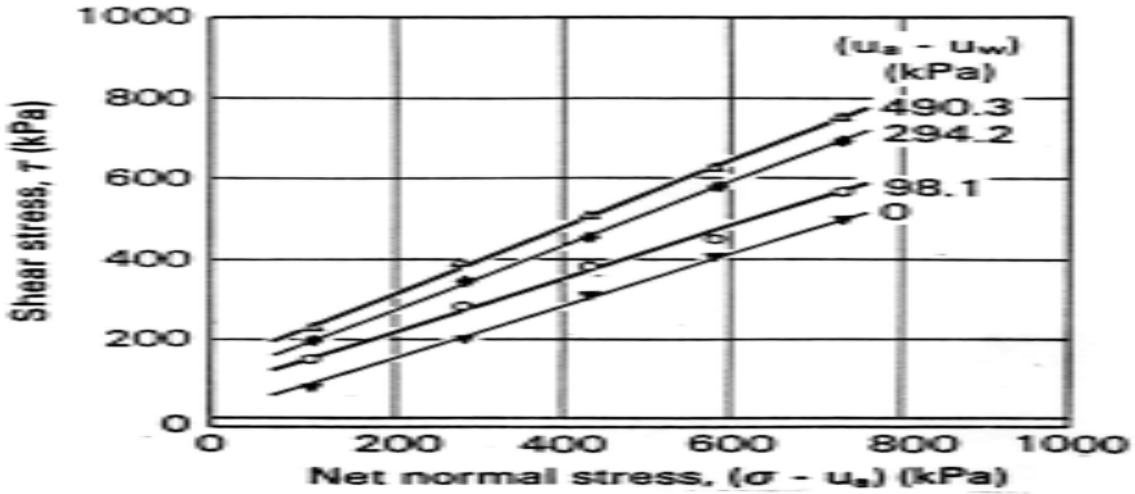

(a) Horizontal projections of the failure envelope onto the τ versus $(\sigma - u_a)$ plane

Curved on the matric suction plane

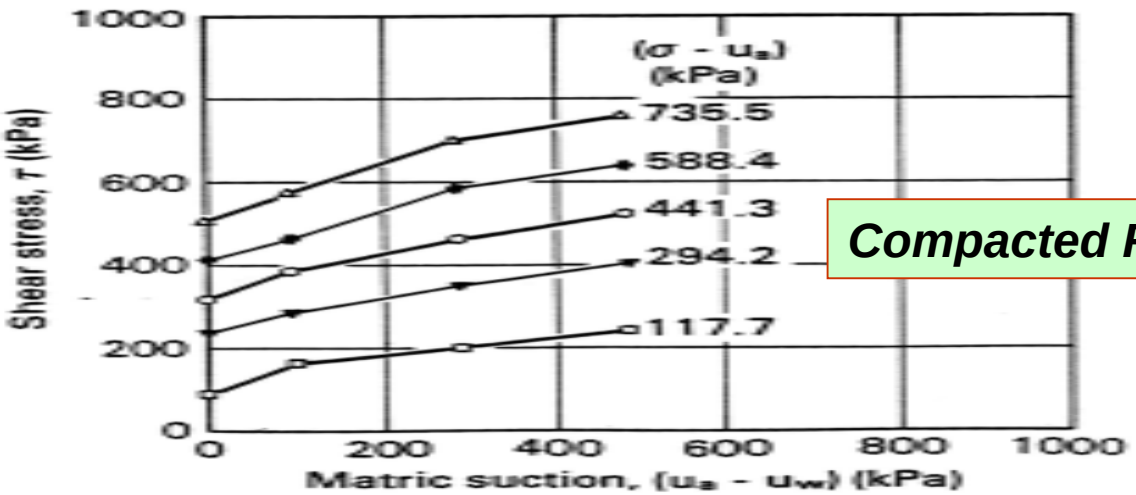

Compacted Red clay

(b) Horizontal projections of the failure envelope onto the τ versus $(u_a - u_w)$ plane

Direct shear tests on compacted red clay of Guadalix de la Sierra (from Escario and Sáez, 1986)

Linear on the Net Normal Stress plane

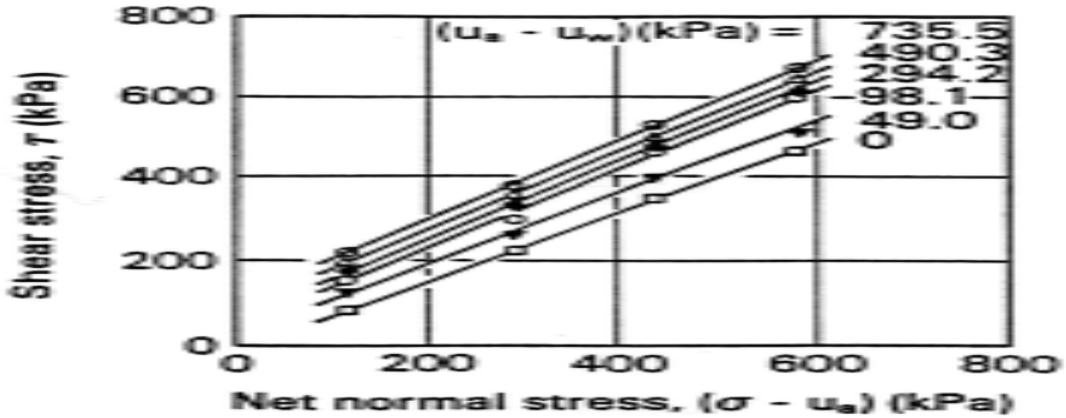

(a) Horizontal projections of the failure envelope onto the shear stress versus $(\sigma - u_a)$ plane

Compacted Madrid clayey sand

Curved on the matric suction plane

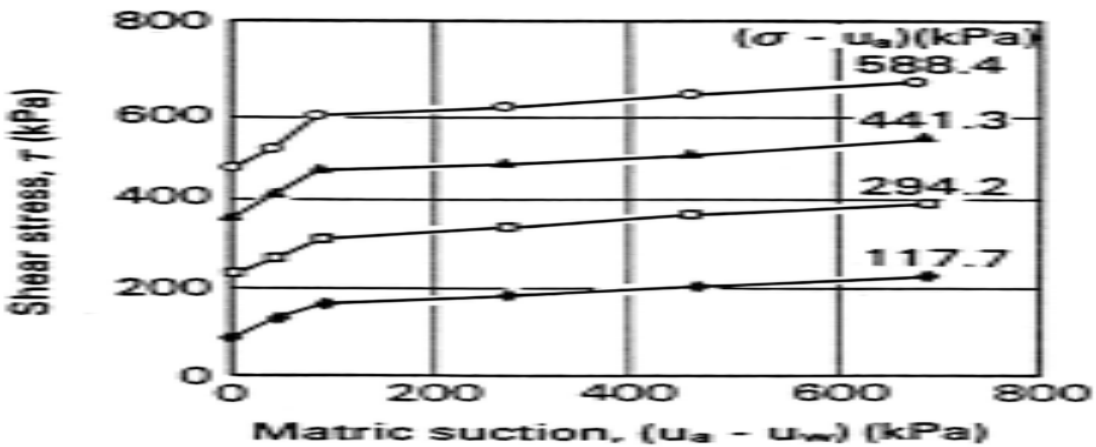

(b) Horizontal projections of the failure envelope onto the shear stress versus $(u_a - u_w)$ plane

Direct shear tests on compacted Madrid clayey sand (from Escario and Sáez, 1986)